

A two-step route to planar perovskite cells exhibiting reduced hysteresis

Alexander H. Ip, Li Na Quan, Michael M. Adachi, Jeffrey J. McDowell, Jixian Xu, Dong Ha Kim, and Edward H. Sargent

Citation: [Applied Physics Letters](#) **106**, 143902 (2015); doi: 10.1063/1.4917238

View online: <http://dx.doi.org/10.1063/1.4917238>

View Table of Contents: <http://scitation.aip.org/content/aip/journal/apl/106/14?ver=pdfcov>

Published by the [AIP Publishing](#)

Articles you may be interested in

[Numerical simulation: Toward the design of high-efficiency planar perovskite solar cells](#)

Appl. Phys. Lett. **104**, 253508 (2014); 10.1063/1.4885367

[Dominating recombination mechanisms in organic solar cells based on ZnPc and C60](#)

Appl. Phys. Lett. **102**, 163901 (2013); 10.1063/1.4802276

[Analyzing carrier lifetime of double-layer organic solar cells by using optical electric-field-induced second-harmonic generation measurement](#)

Appl. Phys. Lett. **98**, 133507 (2011); 10.1063/1.3574002

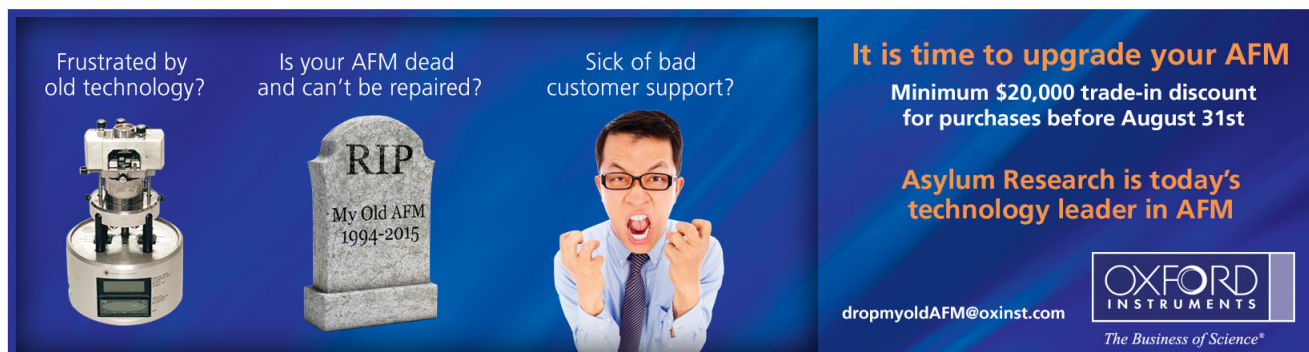
[Complexation of pyrrolidinofullerenes and zinc-phthalocyanine in a bilayer organic solar cell structure](#)

Appl. Phys. Lett. **87**, 244102 (2005); 10.1063/1.2146070

[Fullerenes and nanostructured plastic solar cells](#)

AIP Conf. Proc. **442**, 523 (1998); 10.1063/1.56493

Frustrated by old technology? Is your AFM dead and can't be repaired? Sick of bad customer support?



It is time to upgrade your AFM
Minimum \$20,000 trade-in discount for purchases before August 31st

Asylum Research is today's technology leader in AFM

dropmyoldAFM@oxinst.com

OXFORD INSTRUMENTS
The Business of Science®

A two-step route to planar perovskite cells exhibiting reduced hysteresis

Alexander H. Ip,¹ Li Na Quan,² Michael M. Adachi,¹ Jeffrey J. McDowell,¹ Jixian Xu,¹ Dong Ha Kim,² and Edward H. Sargent^{1,a)}

¹*Department of Electrical and Computer Engineering, University of Toronto, 10 King's College Road, Toronto, Ontario M5S 3G4, Canada*

²*Department of Chemistry and Nano Science, Ewha Womans University, 52, Ewhayeodae-gil, Seodaemun-gu, Seoul 120-750, South Korea*

(Received 9 February 2015; accepted 30 March 2015; published online 7 April 2015)

A simple two-step method was used to produce efficient planar organolead halide perovskite solar cells. Films produced using solely iodine containing precursors resulted in poor morphology and failed devices, whereas addition of chlorine to the process greatly improved morphology and resulted in dense, uniform perovskite films. This process was used to produce perovskite solar cells with a fullerene-based passivation layer. The hysteresis effect, to which planar perovskite devices are otherwise prone, was greatly suppressed through the use of this interface modifier. The combined techniques resulted in perovskite solar cells having a stable efficiency exceeding 11%. This straightforward fabrication procedure holds promise in development of various optoelectronic applications of planar perovskite films. © 2015 AIP Publishing LLC.

[<http://dx.doi.org/10.1063/1.4917238>]

Organolead halide perovskites have garnered significant interest in recent years in light of their rapid rise in photovoltaic (PV) power conversion efficiency (PCE). Building on early reports of promising device performance,^{1–4} the certified efficiency has now reached over 20%.^{5,6} This is comparable to vacuum deposited thin film solar cells (such as CdTe), but, remarkably for such efficiencies, perovskites are amenable to low-temperature solution processing.^{7–9}

Efficient perovskite devices have been developed in many configurations, including both as planar films¹⁰ and with perovskite infiltrated into mesoporous scaffolds of titania,¹¹ alumina,¹² nickel oxide,¹³ or zirconia.¹⁴ These structures have been used with conventional materials stacks on TiO₂ and with organic photovoltaic (OPV) style inverted structures.¹⁵ While the most efficient devices are currently mesoscopic in nature, planar films are of interest due to their relative processing simplicity as well as their potential in other non-PV applications such as photodetection and photoemission. However, one-step processing of uniform and pinhole-free planar films has been found to require stringent processing conditions.¹⁶ A two-step interdiffusion approach has recently been shown to result in high quality films in an OPV-style structure.¹⁷

Unfortunately, planar devices have also been shown to be more susceptible to hysteretic effects^{18,19} which have been attributed to the migration of ions within the perovskite film.^{20,21} The ionic current can arise due to unpassivated trap states that are found at perovskite grain boundaries due to non-ideal formation conditions.²² Various schemes have been developed to reduce the effect of these dangling bonds by application of passivants at the film interfaces^{23,24} and within the film.²⁰ Indeed, fullerenes have been found to passivate these trap states efficiently and reduce hysteresis in perovskite devices.^{20,25,26} Intriguingly, inverted (or OPV

style architecture) perovskite cells typically use fullerenes as an electron extracting layer and tend to have low hysteresis.^{27,28} Here, we aimed to build efficient planar conventional architecture perovskite solar cells through a two-step interdiffusion route using a phenyl-C₆₁-butyric acid methyl ester (PCBM, a fullerene derivative) interfacial layer to reduce hysteresis.

The process used is depicted in Figure 1(a). Fluorine-doped tin oxide (FTO) substrates were coated with a 50 nm TiO₂ compact layer deposited by sputtering in an Angstrom Engineering Åmod deposition system and followed by a TiCl₄ treatment described previously.²⁹ For devices using PCBM interfacial layers, a 10 mg/ml solution of PCBM dissolved in chlorobenzene was cast on top of the TiO₂ at 4000 rpm. PbI₂ was dissolved in dimethylformamide (DMF) to a 0.8 mol/ml concentration and methylammonium iodide (MAI) was dissolved in isopropanol (IPA) at 0.25 mol/ml. Both the substrates and the PbI₂ solution were heated to 65 °C. 80 μl of the PbI₂ precursor was spin-cast onto the hot substrate at 6000 rpm and the film was left to dry at 65 °C for 5 min. The substrate was cooled to room temperature, after which 100 μl of the MAI solution was cast while the substrate was spinning at 3000 rpm. This led immediately to a darkening of the film as perovskite was formed at the interface of the two precursors. To form the perovskite fully, the film was dried at 70 °C for 10 min, then ramped to 90 °C for 15 min, and finally at 125 °C for 12 min to encourage crystal growth.³⁰ Spiro-OMeTAD was dissolved in chlorobenzene at 63 mg/ml and doped using 20 μl/ml of tert-butylpyridine and 70 μl/ml of an acetonitrile solution containing 170 mg/ml bis(trifluoromethane)sulfonimide lithium salt. This solution was filtered and spin-cast at 4000 rpm after the films had cooled. To form the top contacts, 100 nm of gold was deposited through a shadow mask by e-beam evaporation. The electronic structure of the device is displayed in Figure 1(b), with the TiO₂/PCBM serving as the electron-extracting electrode and the Spiro-OMeTAD serving the same purpose for holes.

^{a)}Author to whom correspondence should be addressed. Electronic mail: ted.sargent@utoronto.ca

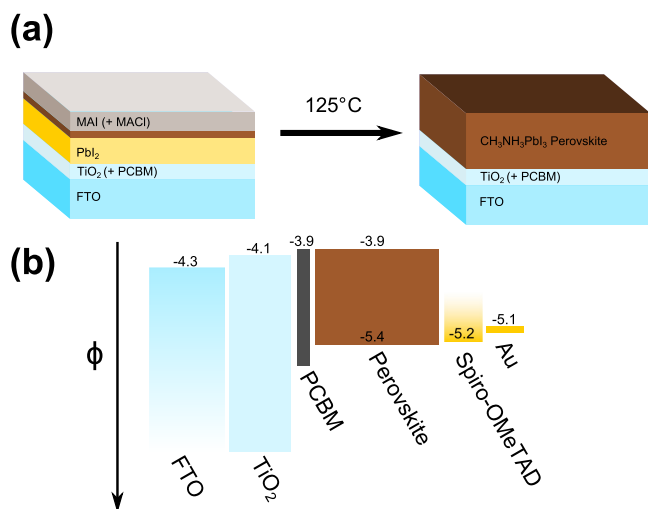


FIG. 1. Fabrication process used in this work. (a) PbI_2 is deposited on the TiO_2 substrate followed by casting of a methylammonium halide solution. Perovskite is formed at the interface between the two layers. Upon annealing, the precursors interdiffuse and the complete perovskite film is formed. (b) Electronic band structure of the device. Electrons are extracted through the TiO_2 , while holes are extracted through the Spiro-OMeTAD layer.

Though perovskite was formed, the films were visibly hazy and in our initial tests the devices were often short-circuited. This suggested that poor morphology was preventing full coverage of each device layer and resulting in non-selective charge carrier extraction.

We used scanning electron microscopy (SEM) to verify this hypothesis. Since the haziness occurred as the MAI solution was deposited, we first inspected a sample immediately

prior to the annealing step. Surprisingly, the film did not consist of a flat MAI layer on top of PbI_2 , as shown in Figure 2(a); instead, large micron-scale protrusions from the surface of the film were observed. These dramatic features are much larger than the combined thickness of the device layers. As seen in the 45° view of Figure 2(c), many of these features are distributed over the film, resulting in large nonuniformity. Rapid reaction of the precursors may lead to perovskite growth over droplets of MAI solution as the IPA is evaporating. In some cases, the solution is pushed upwards as the perovskite grows, leading to the structures seen in Figure 2(a). Following the annealing process, the structures are not as apparent but result in large morphological variations throughout the film, as shown in Figure 2(e).

Since these poor morphologies showed poor performance, we sought to control the crystallization of the film by adding chlorine into the process. The addition of chlorine as a precursor has been shown to improve electronic properties of perovskites, even though it is not detected in the final product.^{22,31,32} Chloride is also known to aid formation of high quality perovskite films by controlling crystallization.^{33,34} We took the view that this would be particularly helpful for the two-step interdiffusion method to maintain uniform growth from the interface between the precursors. We introduced Cl in the form of methylammonium chloride (MACl, prepared according to literature methods).³² A 0.25 mol/ml solution of MACl in IPA was produced and mixed with the MAI solution at a ratio of 2:1 (MAI:MACl). The mixture was then used in place of the MAI solution in the film preparation.

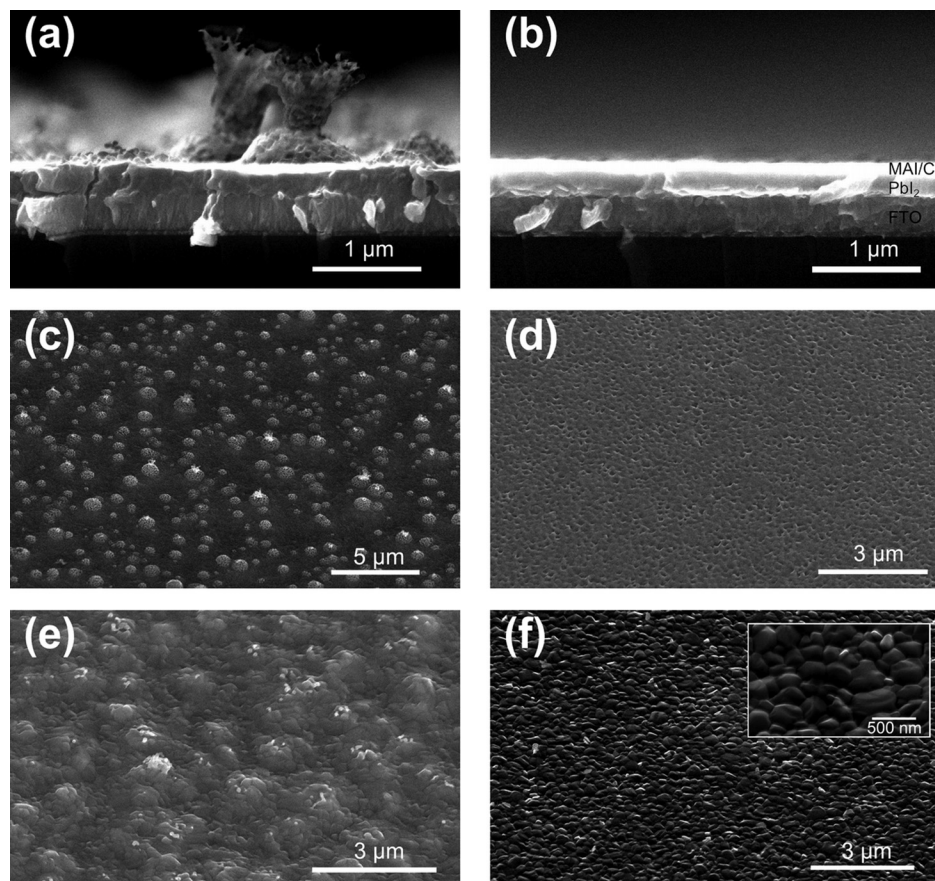


FIG. 2. Scanning electron micrographs of the perovskite films formed with and without chlorine inclusion. (a) and (b) Cross sectional view of the films of PbI_2 and either (a) MAI or (b) MAI and MACl, both prior to annealing. (c) 45° view of the iodide only film prior to annealing. (d) 45° view of the film with chlorine inclusion prior to annealing. (e) 45° view of the iodide only film after annealing. (f) 45° view of the film with chlorine inclusion after annealing. Inset: close-up view to show grains.

Notably, the film formed following deposition of the precursors was specularly reflective, in contrast to the diffuse reflectance of the films prepared using iodine only. SEM of the chloride prepared film, shown in Figure 2(b), showed flat films with no apparent protrusions caused by rapid reaction. The unreacted precursors are apparent and evenly distributed. As seen from the 45° micrograph in Figure 2(d), the film has long range uniformity. Finally, upon annealing, a dense perovskite film is formed, with crystallites in the range of hundreds of nanometers (Figure 2(f)). In sum, through simple addition of a chlorine precursor, the morphology was drastically improved. Absorption and photoluminescence (PL) measurements confirmed that, for both precursor sets, MAPbI₃ perovskite was formed. As seen in Figure S1,³⁵ the absorption onsets for both films are the same, and sharp PL peaks were observed. Notably, the film with MAI precursor had better absorption beyond 550 nm, likely due to the difference in morphology. Indeed, as seen in Figure S2,³⁵ the film formed without chloride varied greatly in thickness as a consequence of the rapid film reaction. MAI inclusion resulted in a generally thinner film, but with long range thickness uniformity.

The improved dense and uniform perovskite films allowed us to build devices with a high yield. We proceeded to build solar cells and observe the effect of a PCBM interlayer. A Keithley 2400 source-meter was used to measure the current density-voltage scans of the devices under AM1.5G simulated solar illumination. Scans were recorded both for increasing and decreasing voltage to observe any hysteretic effects. The stability at the maximum power point (MPP) was determined by measuring the current density while the voltage was held at MPP as determined by the open-circuit to short-circuit scan. The source intensity was measured using a Melles-Griot broadband power meter and spectral mismatch was corrected for using a calibrated reference Si solar cell.

A J-V scan for a device with no PCBM layer is shown in Figure 3(a). It can be seen that there is a large discrepancy between the two scans in different directions due to the lack of passivation. While the open-circuit to short-circuit scan displays good short-circuit current (J_{SC}), open-circuit voltage (V_{OC}), and fill factor (FF), the reverse scan shows significant losses in all of these parameters. In contrast, the device with a PCBM interfacial layer (Figure 3(b)) demonstrates greatly reduced hysteresis.

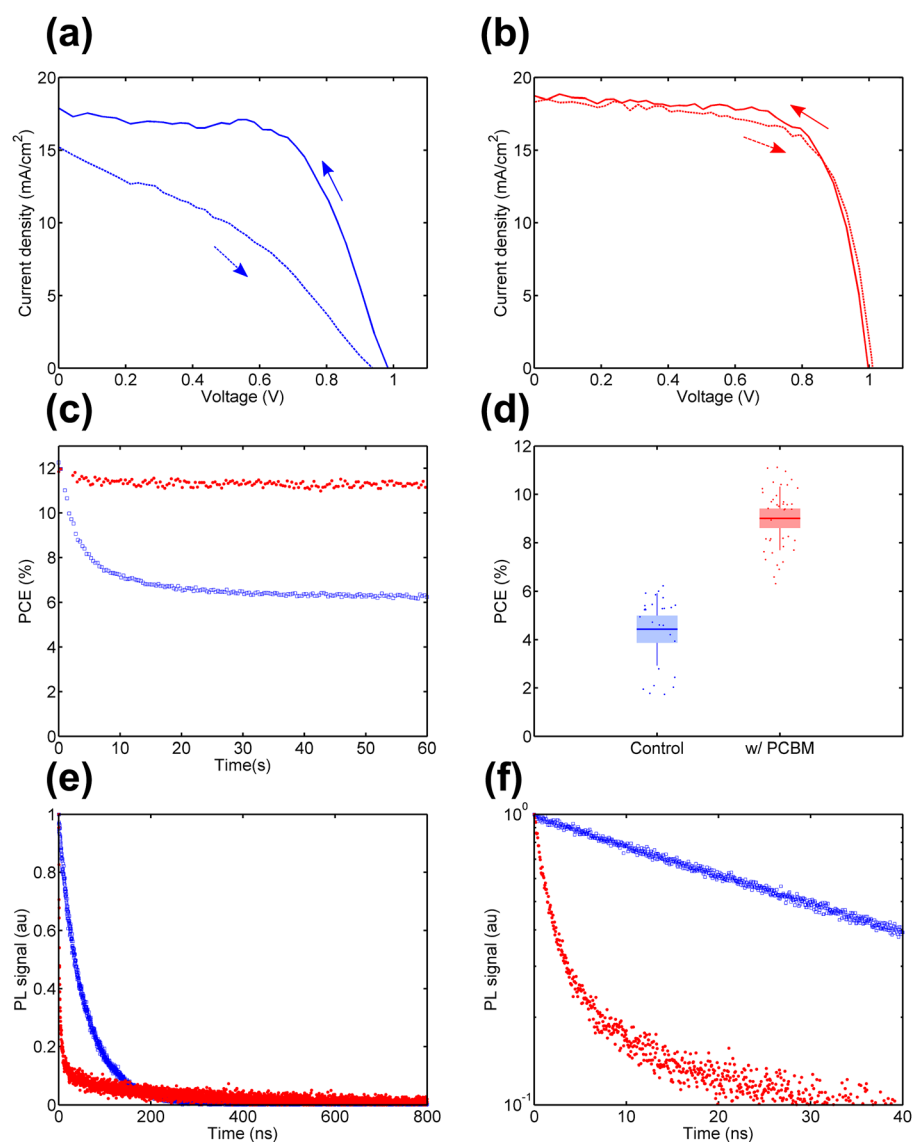


FIG. 3. Device performance of chloride derived perovskite films with and without PCBM layer. (a) J-V scans of a device with no PCBM interfacial layer. The arrows correspond to the scan direction. (b) J-V scans for a device with a PCBM interfacial layer demonstrating reduced hysteresis. (c) Static PCE scan with the voltage held at the MPP voltage. Open blue squares represent the device with no PCBM, while closed red circles indicate the device with PCBM layer. (d) Distribution of device performance. For each box plot, the horizontal line represents the mean of the data set, while the shaded box shows the standard error of the mean. The whiskers represent the standard deviation and each point is a different device. (e) Transient photoluminescence curves at 770 nm emission for perovskite films on TiO₂ with (red circles) and without (open blue squares) PCBM. (f) Semilog plot of transient PL measurements at short time scales to show fast decay behavior.

The operation of a solar cell must be judged not be through J-V scans, but rather through constant power output at MPP conditions. Thus, the efficiency of the cells in Figures 3(a) and 3(b) was measured over time in order to approximate the expected efficiency of an operating device and eliminate the complications of hysteretic J-V curves. The device with no PCBM layer dropped nearly 50% from its initial value before settling at 6.2% PCE. In contrast, the addition of a PCBM interlayer resulted in a very stable PCE output at 11.1% PCE. The PCBM interlayer significantly reduces the hysteresis and leads to high efficiency devices due to improved passivation of the TiO₂/perovskite interface. It is likely that PCBM infiltrates somewhat into the relatively thin (250 nm) perovskite film and thus reduces internal traps while improving electronic extraction.²⁰ The distribution of device performance can be seen in Figure 3(d). Here, we show the PCE of each device based on a static MPP scan to most fairly compare the performance. The use of the passivating PCBM layer increases the mean PCE from 4.4% up to 9.0% over approximately 30 devices.

To better understand the effect that the PCBM layer had on the device performance, we measured time-resolved photoluminescence decay curves (Figures 3(e) and 3(f)) of perovskite films on TiO₂ with and without a PCBM interfacial layer. Measurements were carried out on a Horiba FluoroLog-3 spectrofluorometer using a 504 nm pulsed laser diode excitation source and the emission was monitored at 770 nm. Without PCBM, the decay exhibits single exponential character with a decay time of 43.5 ns. Inclusion of the PCBM layer changes the decay to bi-exponential, with a fast component of 2.1 ns and a slow component of 74.5 ns. The addition of PCBM results in a remarkable increase in PL quenching, indicating very fast electron transfer to the PCBM. This improved extraction can prevent the accumulation of excess capacitive charge that leads to hysteresis.¹⁹ This explanation is supported by the observation of an increased hysteresis appearing at very fast scan rates (Figure S3)³⁵ when settling time is insufficient to eliminate the effect of stored charge. PCBM may also be passivating interface states that trap charge carriers, both at the junction²⁶ and at grain boundaries.²⁰ This result also serves to emphasize the importance of reporting the steady state power output, as in Figure 3(d), in order to avoid transient effects that can obscure actual device performance.

In summary, we have demonstrated a method of producing efficient planar perovskite solar cells with high yield through morphological and interfacial improvements. Addition of a chloride precursor to the film fabrication results in a significantly more uniform film that prevents device short-circuiting. A PCBM passivation layer serves to significantly reduce the hysteresis that plagues many planar perovskite devices and results in a high, stable PCE. Furthermore, the technique should be extendable to other perovskite stoichiometries, including those containing bromide or alternative organic compounds. This work provides a simple route to development of various planar perovskite optoelectronic devices.

This publication was based in part on work supported by Award KUS-11-009-21, made by King Abdullah University of Science and Technology (KAUST), by the Ontario Research Fund Research Excellence Program, and by the

Natural Sciences and Engineering Research Council (NSERC) of Canada. The authors thank A. J. Labelle, L. R. Rollny, A. K. Johnston, B. R. Sutherland, and O. Voznyy for their help throughout the course of this study. L. N. Quan and D. H. Kim acknowledge the financial support by National Research Foundation of Korea Grant funded by the Korean Government (2014R1A2A1A09005656).

- ¹A. Kojima, K. Teshima, Y. Shirai, and T. Miyasaka, *J. Am. Chem. Soc.* **131**, 6050 (2009).
- ²J.-H. Im, C.-R. Lee, J.-W. Lee, S.-W. Park, and N.-G. Park, *Nanoscale* **3**, 4088 (2011).
- ³H.-S. Kim, C.-R. Lee, J.-H. Im, K.-B. Lee, T. Moehl, A. Marchioro, S.-J. Moon, R. Humphry-Baker, J.-H. Yum, J. E. Moser, M. Grätzel, and N.-G. Park, *Sci. Rep.* **2**, 591 (2012).
- ⁴M. M. Lee, J. Teuscher, T. Miyasaka, T. N. Murakami, and H. J. Snaith, *Science* **338**, 643 (2012).
- ⁵N. J. Jeon, J. H. Noh, W. S. Yang, Y. C. Kim, S. Ryu, J. Seo, and S. I. Seok, *Nature* **517**, 476 (2015).
- ⁶*NREL Best Research-Cell Efficiencies*.
- ⁷J. M. Ball, M. M. Lee, A. Hey, and H. J. Snaith, *Energy Environ. Sci.* **6**, 1739 (2013).
- ⁸D. Liu and T. L. Kelly, *Nat. Photonics* **8**, 133 (2014).
- ⁹P. Docampo, J. M. Ball, M. Darwich, G. E. Eperon, and H. J. Snaith, *Nat. Commun.* **4**, 2761 (2013).
- ¹⁰M. Liu, M. B. Johnston, and H. J. Snaith, *Nature* **501**, 395 (2013).
- ¹¹N. J. Jeon, J. H. Noh, Y. C. Kim, W. S. Yang, S. Ryu, and S. I. Seok, *Nat. Mater.* **13**, 897 (2014).
- ¹²T. Leijtens, G. E. Eperon, S. Pathak, A. Abate, M. M. Lee, and H. J. Snaith, *Nat. Commun.* **4**, 2885 (2013).
- ¹³K.-C. Wang, J.-Y. Jeng, P.-S. Shen, Y.-C. Chang, E. W.-G. Diau, C.-H. Tsai, T.-Y. Chao, H.-C. Hsu, P.-Y. Lin, P. Chen, T.-F. Guo, and T.-C. Wen, *Sci. Rep.* **4**, 4756 (2014).
- ¹⁴A. Mei, X. Li, L. Liu, Z. Ku, T. Liu, Y. Rong, M. Xu, M. Hu, J. Chen, Y. Yang, M. Grätzel, and H. Han, *Science* **345**, 295 (2014).
- ¹⁵J. You, Z. Hong, Y. (Michael) Yang, Q. Chen, M. Cai, T.-B. Song, C.-C. Chen, S. Lu, Y. Liu, H. Zhou, and Y. Yang, *ACS Nano* **8**, 1674 (2014).
- ¹⁶G. E. Eperon, V. M. Burlakov, P. Docampo, A. Goriely, and H. J. Snaith, *Adv. Funct. Mater.* **24**, 151 (2014).
- ¹⁷Z. Xiao, C. Bi, Y. Shao, Q. Dong, Q. Wang, Y. Yuan, C. Wang, Y. Gao, and J. Huang, *Energy Environ. Sci.* **7**, 2619 (2014).
- ¹⁸H. J. Snaith, A. Abate, J. M. Ball, G. E. Eperon, T. Leijtens, N. K. Noel, S. D. Stranks, J. T.-W. Wang, K. Wojciechowski, and W. Zhang, *J. Phys. Chem. Lett.* **5**, 1511 (2014).
- ¹⁹H.-S. Kim and N.-G. Park, *J. Phys. Chem. Lett.* **5**, 2927 (2014).
- ²⁰J. Xu, A. Buin, A. H. Ip, W. Li, O. Voznyy, R. Comin, M. Yuan, S. Jeon, Z. Ning, J. McDowell, P. Kanjanaboos, J.-P. Sun, X. Lan, L. N. Quan, D. H. Kim, I. G. Hill, P. Maksymovych, and E. H. Sargent, "Perovskite-Fullerene Hybrid Materials Eliminate Hysteresis in Planar Diodes." *Nat. Commun.* (to be published).
- ²¹W. Tress, N. Marinova, T. Moehl, S. M. Zakeeruddin, M. K. Nazeeruddin, and M. Grätzel, *Energy Environ. Sci.* **8**, 995–1004 (2015).
- ²²A. Buin, P. Pietsch, J. Xu, O. Voznyy, A. H. Ip, R. Comin, and E. H. Sargent, *Nano Lett.* **14**, 6281 (2014).
- ²³A. Abate, M. Saliba, D. J. Hollman, S. D. Stranks, K. Wojciechowski, R. Avolio, G. Grancini, A. Petrozza, and H. J. Snaith, *Nano Lett.* **14**, 3247 (2014).
- ²⁴N. K. Noel, A. Abate, S. D. Stranks, E. S. Parrott, V. M. Burlakov, A. Goriely, and H. J. Snaith, *ACS Nano* **8**, 9815 (2014).
- ²⁵Y. Shao, Z. Xiao, C. Bi, Y. Yuan, and J. Huang, *Nat. Commun.* **5**, 5784 (2014).
- ²⁶K. Wojciechowski, S. D. Stranks, A. Abate, G. Sadoughi, A. Sadhanala, N. Kopidakis, G. Rumbles, C.-Z. Li, R. H. Friend, A. K.-Y. Jen, and H. J. Snaith, *ACS Nano* **8**, 12701 (2014).
- ²⁷S. Bai, Z. Wu, X. Wu, Y. Jin, N. Zhao, Z. Chen, Q. Mei, X. Wang, Z. Ye, T. Song, R. Liu, S. Lee, and B. Sun, *Nano Res.* **7**, 1749 (2014).
- ²⁸J. Seo, S. Park, Y. C. Kim, N. J. Jeon, J. H. Noh, S. C. Yoon, and S. I. Seok, *Energy Environ. Sci.* **7**, 2642 (2014).
- ²⁹A. H. Ip, S. M. Thon, S. Hoogland, O. Voznyy, D. Zhitomirsky, R. Debnath, L. Levina, L. R. Rollny, G. H. Carey, A. Fischer, K. W. Kemp, I. J. Kramer, Z. Ning, A. J. Labelle, K. W. Chou, A. Amassian, and E. H. Sargent, *Nat. Nanotechnol.* **7**, 577 (2012).
- ³⁰M. Saliba, K. W. Tan, H. Sai, D. T. Moore, T. Scott, W. Zhang, L. A. Estroff, U. Wiesner, and H. J. Snaith, *J. Phys. Chem. C* **118**, 17171 (2014).

- ³¹S. D. Stranks, G. E. Eperon, G. Grancini, C. Menelaou, M. J. P. Alcocer, T. Leijtens, L. M. Herz, A. Petrozza, and H. J. Snaith, *Science* **342**, 341 (2013).
- ³²P. Docampo, F. C. Hanusch, S. D. Stranks, M. Döblinger, J. M. Feckl, M. Ehrensperger, N. K. Minar, M. B. Johnston, H. J. Snaith, and T. Bein, *Adv. Energy Mater.* **4**, 1400355 (2014).

- ³³S. T. Williams, F. Zuo, C.-C. Chueh, C.-Y. Liao, P.-W. Liang, and A. K.-Y. Jen, *ACS Nano* **8**, 10640 (2014).
- ³⁴Y. Zhao and K. Zhu, *J. Phys. Chem. C* **118**, 9412 (2014).
- ³⁵See supplementary material at <http://dx.doi.org/10.1063/1.4917238> for additional absorption, PL, SEM micrographs, and J-V curves at varying scan speed.